Japanese Journal of Applied Physics 55, 05FD12 (2016)
http://doi.org/10.7567/JJAP.55.05FD12

REGULAR PAPER

High-quality InN films on GaN using graded InGaN buffers by MBE

SM Islam[1], Vladimir Protasenko[1], Sergei Rouvimov[2], Huili (Grace) Xing[1,3], and Debdeep Jena[1,3*]

[1]School of Electrical and Computer Engineering, Cornell University, Ithaca, NY 14853, U.S.A.
[2]Notre Dame Integrated Imaging Facility, University of Notre Dame, IN 46556, U.S.A.
[3]Department of Materials Science and Engineering, Cornell University, Ithaca, NY 14853, U.S.A.

*E-mail: djena@cornell.edu

Received December 6, 2015; revised February 15, 2016; accepted February 17, 2016; published online April 25, 2016

The growth of high-quality thick InN films is challenging because of the lack of native substrates. In this work, we demonstrate the use of a linearly graded InGaN buffer layer for the growth of InN films on GaN substrates. A 500 nm InN film with <0.1 nm RMS roughness is obtained with a peak mobility of 1410 $cm^2/(V{\cdot}s)$ at 300 K. A strong room temperature photoluminescence showing a bandgap of 0.65 eV with 79 meV linewidth is observed. A graded InGaN buffer is found to lead to extremely smooth and high-quality InN films. © 2016 The Japan Society of Applied Physics

1. Introduction

There is significant interest in InN because of the small bandgap and effective mass.[1–6] Room-temperature electron mobilities in the range of 14,000 $cm^2/(V{\cdot}s)$ and a high saturation velocity of 5×10^7 cm/s are expected in pristine InN.[7–9] These properties can make it attractive for high-speed electronic applications and infrared optical devices.[10–13] Many reports have been published on the high-quality crystal growth of InN using metal organic CVD (MOCVD) and MBE.[14–24] MBE is preferred over MOCVD because of the low dissociation temperature (~500 °C) of InN.[16,25] Owing to the lack of native substrates, InN is typically grown on GaN[17,26,27] with a 11% lattice mismatch, resulting in dislocation densities (DDs) of $\sim 5 \times 10^{11}$ cm^{-2}.[17] Electron scattering from these dislocations plays a dominant role in the measured low mobility of ~1000 $cm^2/(V{\cdot}s)$[17] for InN films of <1 µm, compared with theoretical limits. By growing 5-µm-thick InN films, DD was reduced and a record mobility of ~3200 $cm^2/(V{\cdot}s)$ was achieved.[27] A common approach to reducing DD on foreign substrates is to use a buffer layer. Different buffer layers such as low-temperature (LT) GaN,[28] AlN,[15] and LT InN[29] have been experimentally investigated. Yet there is room for improving the crystal quality, surface smoothness, and measured mobility of thick InN films with buffer layers.

In this work, we experimentally demonstrate a new buffer layer approach to growing thick (500 nm) InN films on GaN substrates. A linearly graded $Ga_xIn_{1-x}N$ (x: 1 → 0) layer is inserted between epitaxial InN and GaN to accommodate the 11% lattice mismatch. The crystal quality was characterized by high-resolution X-ray diffraction (HR-XRD) analysis and transmission electron microscopy (TEM). Optical properties were investigated with photoluminescence (PL). Surface properties were studied using atomic force microscopy (AFM) and the electronic transport properties were analyzed using Hall measurements. A control sample was grown with an LT InN buffer layer[29] and used to compare the electronic and optical properties with the new graded (GR) buffer approach.

2. Experimental methods

A nitrogen-plasma-assisted Veeco Gen-930 MBE system was used for all growth processes reported here. The structures were grown on semi-insulating GaN templates on SiC. A 3-in. wafer was diced into 1×1 cm^2 pieces, mounted on a Si wafer using indium, and solvent-cleaned to remove surface contaminants before loading into the MBE entry chamber. Two sets of bakes were performed at 200 °C (7 h) and 450 °C (1.5 h) in the entry and buffer chamber respectively. The samples were then transferred into the growth chamber loaded with Ga and In effusion cells, and a N_2 plasma source. A plasma power of 400 W was used for all growth processes corresponding to a growth rate of ~300 nm/h. The chamber pressure was maintained at $\sim 2.1 \times 10^{-5}$ Torr during all growths by providing a constant N_2 flow of 0.9 sccm. Since the InN surface temperature is extremely important[26] for the good control of growth, a pyrometer was used to measure the surface temperature in addition to the thermocouple temperature. Thermocouple readings are reported here unless mentioned otherwise. A 10 rpm rotation was used during the growth, and in-situ reflection high energy electron diffraction (RHEED) was used to monitor the surface growth conditions.

After growth, the mounting indium metal on the back side of the samples, as well as any excess indium droplets on the surface was removed by treatment with HCl for 20 min before further measurements.

Two sets of samples were grown and investigated in this work: both samples had ~500 nm InN films on top, but for one a LT InN buffer was used, and a linearly graded GaInN buffer was used for the other. As shown in the schematic in Fig. 1, a 50-nm-thick GaN layer was first grown on the GaN template. Then, a ~80 nm buffer layer was used for both samples, followed by a 500-nm-thick InN film. To ensure a smooth surface, a metal-rich growth condition was maintained throughout. For the LT InN buffer samples, after growing GaN, the substrate was cooled down to 350 °C to grow the InN layer. This 350 °C thermocouple temperature corresponded to the ~420 °C pyrometer temperature. After the 80 nm LT InN buffer growth, the substrate temperature was increased to 375 °C (~460 °C pyrometer temperature) to deposit a thick InN film. On the other hand, for the graded GaInN buffer samples as shown in Fig. 1(b), after growing 50 nm GaN, a linearly graded $Ga_xIn_{1-x}N$ (x: 1 → 0) layer was grown. The substrate temperature was linearly reduced from 600 to 375 °C for this layer. To change the composition of the GaInN buffer linearly with position, a computer program was used to control the indium and gallium cell temperatures and the corresponding fluxes. This is shown in the growth diagram of Fig. 1(b).

 © 2016 The Japan Society of Applied Physics

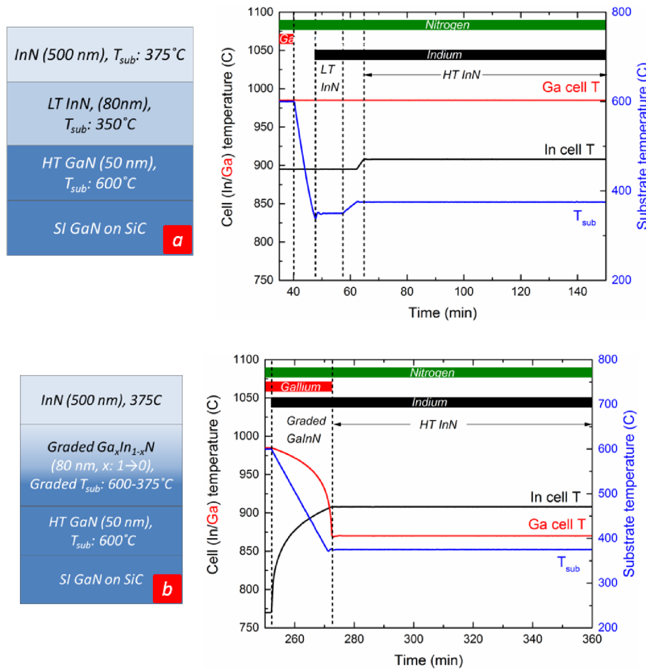

Fig. 1. (Color online) Schematic structure and growth diagram for (a) LT InN and (b) GR InGaN buffer samples.

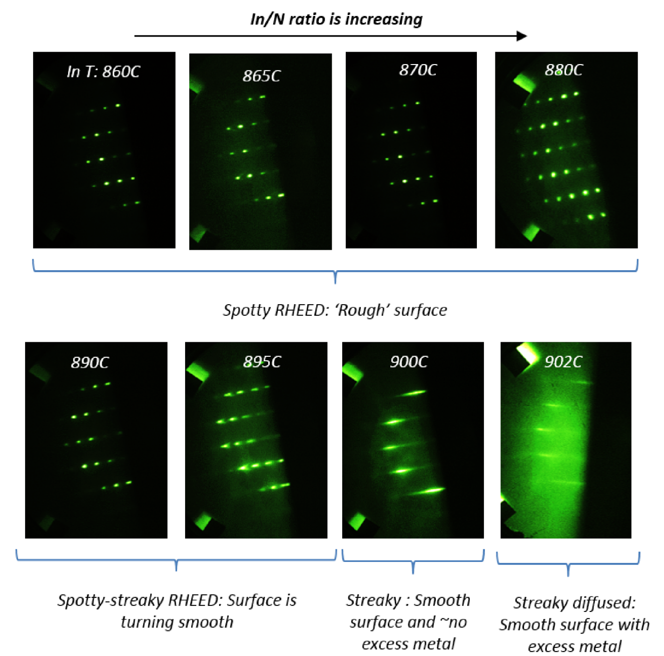

Fig. 2. (Color online) Indium flux optimization study: evolution of RHEED streaks with increase in In/N ratio, from N-rich "spotty" RHEED towards metal-rich "streaky" RHEED.

As discussed in several reports,[26] the surface morphology is very sensitive to the In/N ratio. InN is sensitive to exposure to nitrogen plasma at the growth temperature.[26] When grown under N_2-rich conditions, the surface becomes rough, manifested by spotty RHEED patterns. Metal-rich growth conditions lead to the accumulation of a significant amount of indium on the growth surface. Thus, before proceeding with the two buffer layer experiments, a careful study was performed to optimize the In/N ratio for the growth of the thick InN film to keep the surface smooth, and to simultaneously maintain a low level of excess indium on the surface. For this set of study, eight samples were grown with a 400-nm-thick InN film using a LT InN buffer [Fig. 1(a)] with varying indium flux over a beam equivalent pressure (BEP) range of $(1\text{–}3) \times 10^{-7}$ Torr. The RHEED was monitored during growth. As shown in Fig. 2, with the indium cell being maintained at 860–880 °C [indium flux of $(1\text{–}2) \times 10^{-7}$ Torr] the RHEED was spotty, suggesting a rough surface. As the In cell temperature was increased to 895 °C, the RHEED turned spotty-streaky, indicating the smoothening of the surface. At even higher In cell temperatures, a metal-rich growth regime was attained at 902 °C with an In flux of $\sim 3 \times 10^{-7}$ Torr. The metal-rich condition was manifested by a streaky-diffused RHEED pattern. The RMS roughness measured by AFM revealed a general trend and a one-to-one correlation among the In/N ratio, RHEED pattern streakiness, and surface roughness. The sample grown with the highest indium cell temperature of 902 °C showed the smallest roughness of ~1 nm over a $2 \times 2\,\mu m^2$ area.

On the basis of this study of indium flux, the two samples shown in Fig. 1 were grown under metal-rich InN growth conditions for the topmost thick InN layer. In the following sections, the best representative data are presented over several growth processes. Figure 3 shows the RHEED streaks after growth and the corresponding AFM images of the two samples. The slightly diffused RHEED streaks suggested some residual indium on the surface. This was confirmed by optical microscopy images after taking the samples out of the growth chamber. For the LT buffer sample [Fig. 3(a)], an ~0.98 nm RMS roughness over a $2 \times 2\,\mu m^2$ area was measured, reducing to ~0.274 nm for a $1 \times 1\,\mu m^2$ area scan. For the graded buffer sample, the InN surface was extremely smooth for both large and small area scans. Over a $2 \times 2\,\mu m^2$ area, the RMS roughness was 0.18 nm and, for a $0.5 \times 0.5\,\mu m^2$ area scan, it was 0.08 nm. Such smooth InN surfaces were not observed for any of the growth processes using the LT buffer layer.

3. Results and discussion

The structural quality of the InN films was analyzed by HR-XRD measurements. The (002) ω–2θ triple axis scans for the buffer samples are shown in Fig. 4(a). Strong peaks from SiC, GaN, and InN are seen. For the GR buffer sample, the graded InGaN layer between GaN and InN peaks is evident. The background XRD intensity is shown with a horizontal dotted line that corresponds to the absence of measurable signals from the samples. The measured intensity between the strong InN and GaN peaks reaches this background level for the LT buffer sample. For the GR buffer sample, the presence of the graded layer is manifested by the increased signal intensity compared with the background level between the InN and GaN peaks. A relatively higher intensity of around 16.5° suggests deviation from the ideal linear grading probably due to the phase segregation of InGaN. This linearly graded composition was further confirmed by energy dispersive X-ray (EDX) spectral scan in TEM (Fig. 5). The amount of strain can be extracted from the (002) triple axis data. As shown in Fig. 4(a), the horizontal separation of the peak positions for the InN films suggests the difference in strain among the two samples. To quantify the in-plane and out-of plane strain components, the reciprocal-space maps (RSMs) measured for both samples are shown in Fig. 6. For

 © 2016 The Japan Society of Applied Physics

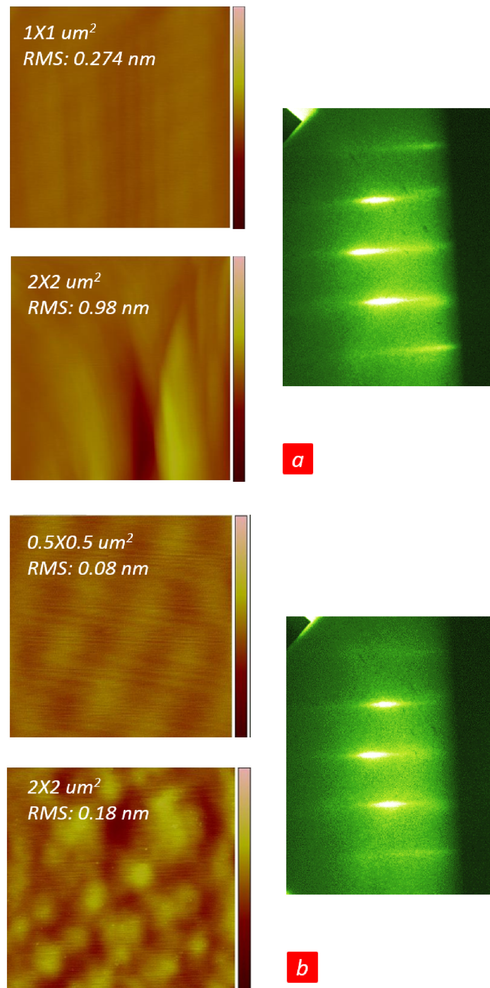

Fig. 3. (Color online) One-to-one correspondence between RHEED and surface roughness for (a) LT InN and (b) GR InGaN buffer samples. Small area scan for GR buffer growth shows an RMS roughness <0.1 nm.

the LT buffer sample, the strains for the in-plane $[(a - a_0)/a_0]$ and the out-of plane $[(c - c_0)/c_0]$ values were measured to be +0.2 and −0.22%, respectively, suggesting a small amount of tensile strain. The red circles show positions for fully relaxed GaN and InN.[29,30] Similarly for the GR buffer, the in-plane strain was −0.08%, and the out-of plane strain was +0.3%, meaning that InN film was partially compressively strained on top of the GR buffer. The difference in the amount of strain is prominent in the change in the c-parameter for the two samples and this agrees with the observation in Fig. 4(a). Similar tensile and compressive strains in the thick InN films have been reported and correlated to the nucleation of the InN films.[31] It was concluded that a N_2-rich three-dimensional (3D) nucleation of the InN films induces tensile strain even for a thickness >5 μm for the top InN film and eventually produces cracks. The nucleation of the LT buffer sample falls into this category of N_2-rich 3D nucleation [Fig. 1(a)]. On the contrary, as long as the 2D nucleation and growth of the layer are maintained, which is the case for the GR buffer, compressive strain can be accommodated in the thick InN films. This suggests that the total misfit DD can be lower for the GR layer sample than for the LT buffer. Figures 4(b) and 4(c) show the comparison of symmetric/asymmetric rocking curves between LT and GR buffer samples. The symmetric

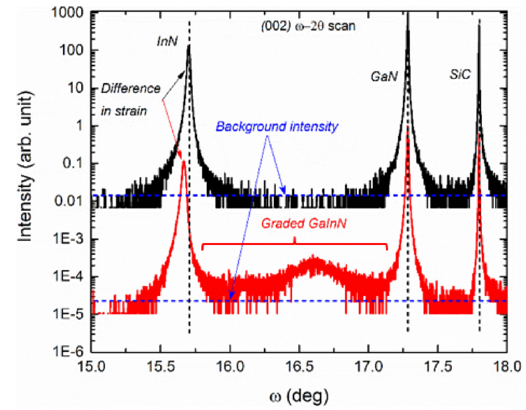

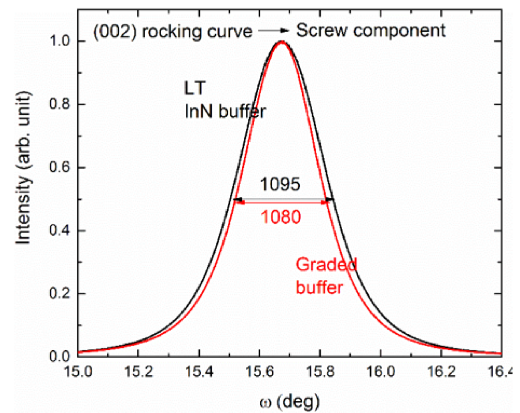

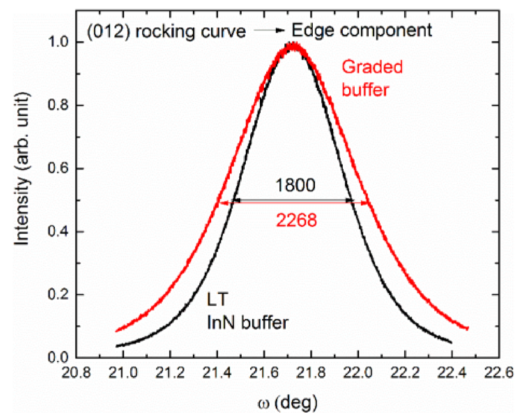

Fig. 4. (Color online) Results of HR-XRD analysis: (a) (002) ω–2θ triple axis scan for both buffer samples showing distinct InN, GaN, and SiC peaks, (b) (002) and (c) (012) rocking curves for comparing screw and edge dislocation components in the InN films for both buffer samples. FWHM values are in arcsec.

(asymmetric) FWHM of the rocking curve gives information about the screw (edge) component of the threading dislocations. By comparing the two buffer schemes, we see that the GR buffer has slightly less screw components but slightly more edge components than the LT buffer. These FWHM values of ~0.27° (~0.5°) for the symmetric (asymmetric) rocking curve measurements are significantly less than those mentioned in Ref. 32 with LT InN buffer, suggesting an improved InN crystal quality.

 © 2016 The Japan Society of Applied Physics

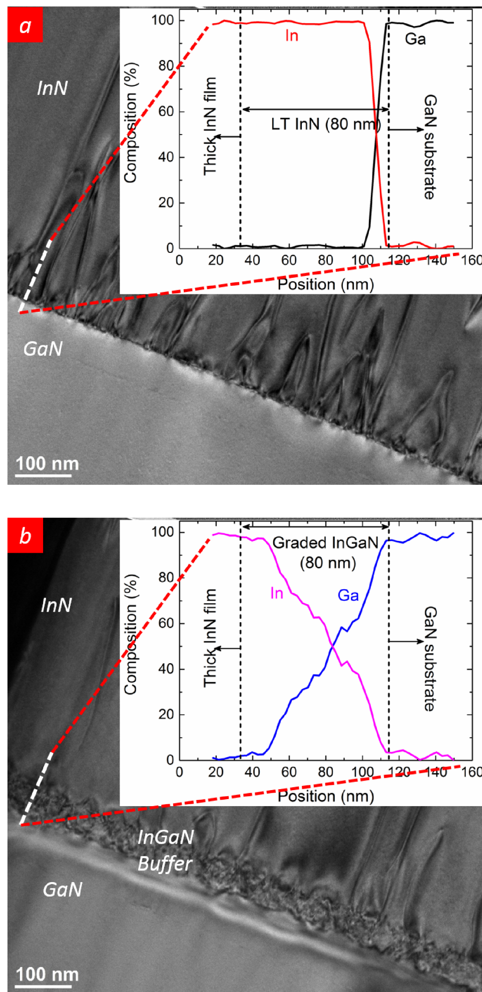

Fig. 5. (Color online) HRTEM and EDX spectra for (a) LT InN and (b) GR buffer samples. The linear grading in In and Ga compositions is verified by the comparative EDX (insets) profiles.

The optical properties of the InN films were analyzed using PL experiments with a 1310 nm laser excitation. Strong 300 K PL signals were measured for both samples. As shown in Fig. 7, 1892 nm (0.655 eV) and 1886 nm (0.657 eV) dominant peaks were observed for the LT InN and GR buffer samples respectively. The FWHM linewidth was narrow and less than 0.1 eV. The observation of PL at room temperature with relatively narrow linewidth suggests the high crystalline quality of the grown InN films. The slightly blue-shifted PL peak for the GR buffer is attributed to the difference in strain on the thick InN films between the samples, which is in agreement with the RSM-based stain measurements. Also the linewidth was smaller for the GR buffer by 5 meV.

To study the electronic transport properties of the grown films, Hall-effect measurement was performed at 300 and 77 K. A drive current of 1 mA was used to measure the Hall data. The measured sheet resistance was ~55 Ω/sq for both samples. A mobility of 1700 (1810) $cm^2/(V\cdot s)$ was measured for the LT buffer at 300 K (77 K). For the GR buffer, the mobility was 1410 (1980) $cm^2/(V\cdot s)$. Significant improvement of the mobility (40%) at 77 K for the GR buffer indicates that the transport in the InN layer is superior to that in the graded InGaN layer. On the other hand, for the LT buffer, the temperature dependence of the mobility is

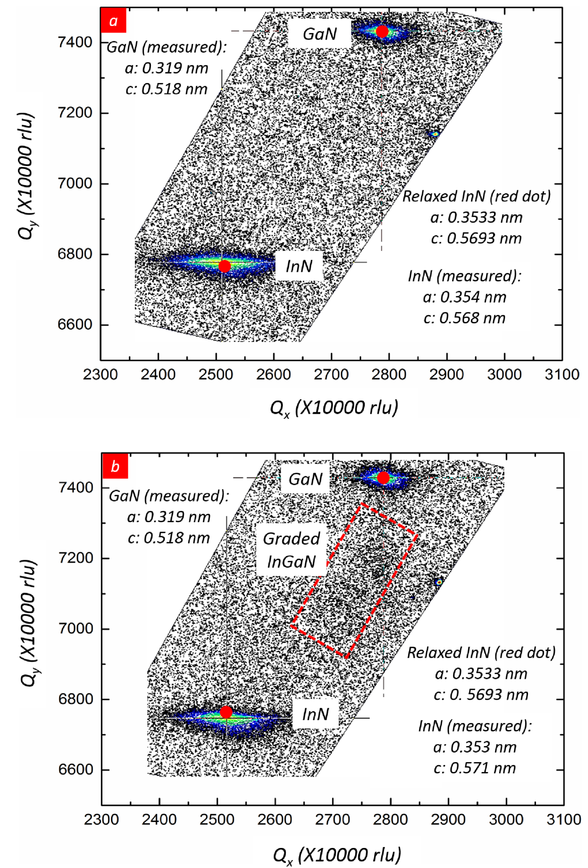

Fig. 6. (Color online) Extraction of in-plane and out-of plane strain components from measured lattice parameters using reciprocal space map for (a) LT and (b) GR buffer samples. The fully relaxed InN/GaN RSM coordinates are marked with red circles.

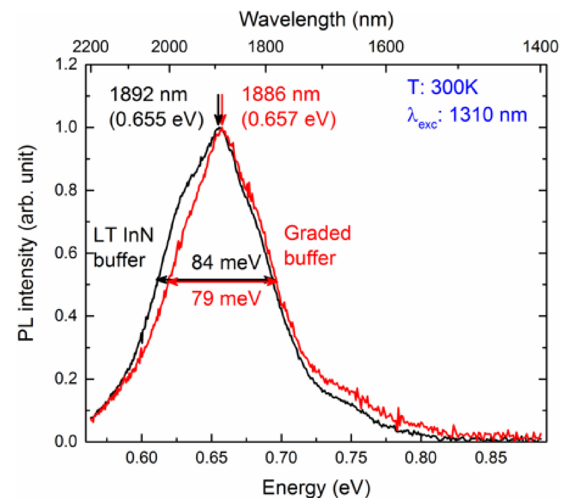

Fig. 7. (Color online) Photoluminescence spectra for both buffer layers measured at 300 K with a 1310 nm laser. The linewidths are shown explicitly for each case.

small (~7%). The sheet charge concentration is of the n type and is determined to be 6.6×10^{13} and $8.1 \times 10^{13}\,cm^{-2}$ for the LT and GR buffer samples, respectively. If the surface accumulation of electrons[33] is ignored, these values correspond to bulk doping densities of 1.29×10^{18} and $1.42 \times 10^{18}\,cm^{-3}$, respectively.

Finally, TEM analysis was performed on the samples. Figure 8(a) shows the high-angle annular dark-field scanning

© 2016 The Japan Society of Applied Physics

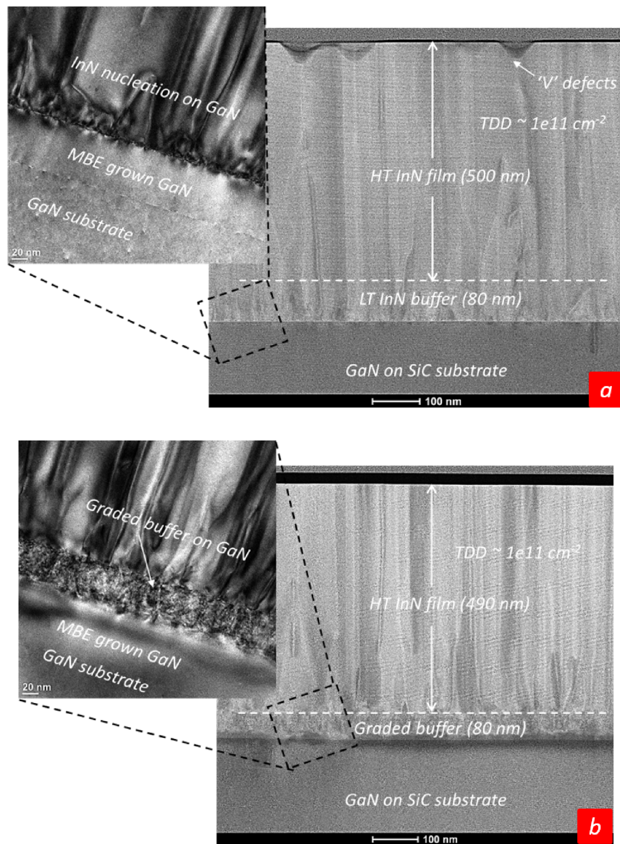

Fig. 8. (Color online) HAADF-STEM images showing the grown thick InN films for (a) LT and (b) GR buffer samples. The zoomed-in HRTEM image shows the nucleation and generation of defects within the buffer layers.

transmission electron microscopy (HAADF-STEM) image of the LT buffer sample. The surface terminates with many "V" defects as seen typically in such growth.[34] The nucleation on the GaN substrate is shown in a zoomed HRTEM image. It was observed that the InN nucleation was very defective owing to a large lattice mismatch (~11%). The total DD near the top of the surface was $\sim 1 \times 10^{11}\,\text{cm}^{-2}$. For the GR buffer sample, Fig. 8(b) shows that the surface was very smooth on the top, which validates what was observed in AFM images. The nucleation layer was very defective in the graded InGaN layer. The total dislocation densities of the buffer layers were similar near the top InN surface. Each of the TD components of the LT and GR buffer samples was estimated from HRTEM images by proper alignment with g vectors. The edge and screw component densities of dislocations for the LT buffer sample were 5×10^{10} and $6 \times 10^{9}\,\text{cm}^{-2}$. For the GR buffer sample, they were measured to be 1.13×10^{11} and $4 \times 10^{9}\,\text{cm}^{-2}$ respectively. These measurements agree with the trend observed by XRD ω rocking curve analysis. The Hall mobility temperature dependence is likely related to the presence of >2× edge components of TDs for the graded buffer sample. Edge TDs are typically charged and cause strong electron scattering. Electron scattering from charged dislocations in the InN film acts as the dominant factor limiting the mobility over the 10–300 K window.[17] The second dominant limiting factor is the presence of ionized impurities. Near the higher end of this temperature window especially around 300 K, optical phonon-assisted scattering further limits the mobility. The low-temperature mobility is determined primarily by charged dislocation scattering. The ~40% increase of the 77 K mobility for the GR buffer can be due to a lower charged dislocation scattering than that for the LT buffer. However, a quantitative analysis and more measurements are necessary to support this claim. A quantitative analysis needs to take into account the fact that there are several layers of carriers with different mobilities: very low mobility electrons at the GaN/InN or graded InGaN layer, and increased mobility electrons towards the surface. Such carefully designed measurements will be performed in the future.

4. Conclusions

A linearly graded InGaN buffer layer was investigated for the growth of thick InN films on GaN. 500-nm-thick InN films were grown with high crystal quality and very smooth surface morphologies. The structural, electronic, and optical properties of the grown InN films on this proposed buffer layer were compared with those of conventional low-temperature InN buffer schemes. The comparative study showed that with similar defect densities and Hall mobilities, the new proposed buffer scheme can lead to a very smooth surface finish without any V defects. By growing thicker InN films (>2 μm), the mobility can be further improved by the annihilation of threading edge dislocations while maintaining a smooth surface that is essential for various devices.

Acknowledgment

The authors would like to thank Tatyana Orlova of the Notre Dame Integrated Imaging Facility, Notre Dame, IN, U.S.A. for help with the TEM sample preparation.

1) J. Wu and W. Walukiewicz, Superlattices Microstruct. **34**, 63 (2003).
2) X. Wang and A. Yoshikawa, Prog. Cryst. Growth Charact. Mater. **48–49**, 42 (2004).
3) V. Yu. Davydov, A. A. Klochikhin, R. P. Seisyan, V. V. Emtsev, S. V. Ivanov, F. Bechstedt, J. Furthmüller, H. Harima, A. V. Mudryi, J. Aderhold, O. Semchinova, and J. Graul, Phys. Status Solidi B **229**, r1 (2002).
4) Y. Ishitani, W. Terashima, S. B. Che, and A. Yoshikawa, Phys. Status Solidi C **3**, 1850 (2006).
5) J. Wu, W. Walukiewicz, K. M. Yu, J. W. Arger, III, E. E. Haller, H. Lu, W. J. Schaff, Y. Saito, and Y. Nanishi, Appl. Phys. Lett. **80**, 3967 (2002).
6) T. Matsuoka, H. Okamoto, M. Nakao, H. Harima, and E. Kurimoto, Appl. Phys. Lett. **81**, 1246 (2002).
7) V. M. Polyakov and F. Schwierz, Appl. Phys. Lett. **88**, 032101 (2006).
8) B. E. Foutz, S. K. O'Leary, M. S. Shur, and L. F. Eastman, J. Appl. Phys. **85**, 7727 (1999).
9) B. R. Nag, J. Cryst. Growth **269**, 35 (2004).
10) H. Lu, W. J. Schaff, J. Hwang, H. Wu, W. Yeo, A. Pharkya, and L. F. Eastman, Appl. Phys. Lett. **77**, 2548 (2000).
11) H. Lu, W. J. Schaff, L. F. Eastman, and C. E. Stutz, Appl. Phys. Lett. **82**, 1736 (2003).
12) J. Wu, W. Walukiewicz, W. Shan, K. M. Yu, J. W. Ager, III, S. X. Li, E. E. Haller, H. Lu, and W. J. Schaff, J. Appl. Phys. **94**, 4457 (2003).
13) Y. Nanishi, Y. Saito, and T. Yamaguchi, Jpn. J. Appl. Phys. **42**, 2549 (2003).
14) R. S. Q. Fareed, R. Jain, R. Gaska, M. S. Shur, J. Wu, W. Walukiewicz, and M. A. Khan, Appl. Phys. Lett. **84**, 1892 (2004).
15) H. Lu, W. J. Schaff, J. Hwang, H. Wu, G. Koley, and L. F. Eastman, Appl. Phys. Lett. **79**, 1489 (2001).
16) C. S. Gallinat, G. Koblmuller, J. S. Brown, S. Bernardis, J. S. Speck, G. D. Chern, E. D. Readinger, H. Shen, and M. Wraback, Appl. Phys. Lett. **89**, 032109 (2006).
17) K. A. Wang, Y. Cao, J. Simon, J. Zhang, A. Mintairov, J. Merz, D. Hall, T. Kosel, and D. Jena, Appl. Phys. Lett. **89**, 162110 (2006).
18) N. Miller, E. E. Haller, G. Koblmuller, C. Gallinat, J. S. Speck, W. J. Schaff,

© 2016 The Japan Society of Applied Physics

M. E. Hawkridge, K. M. Yu, and J. W. Ager, III, Phys. Rev. B **84**, 075315 (2011).
19) G. Koblmüller, C. S. Gallinat, S. Bernardis, J. S. Speck, G. D. Chern, E. D. Readinger, H. Shen, and M. Wraback, Appl. Phys. Lett. **89**, 071902 (2006).
20) L. F. Piper, T. D. Veal, C. F. McConville, H. Lu, and W. J. Schaff, Appl. Phys. Lett. **88**, 252109 (2006).
21) X. Wang, S.-B. Che, Y. Ishitani, and A. Yoshikawa, J. Appl. Phys. **99**, 073512 (2006).
22) N. Khan, A. Sedhain, J. Li, J. Y. Lin, and H. X. Jiang, Appl. Phys. Lett. **92**, 172101 (2008).
23) R. E. Jones, S. X. Li, E. E. Haller, H. C. M. van Genuchten, K. M. Yu, J. W. Ager, III, Z. L. Weber, W. Walukiewicz, H. Lu, and W. J. Schaff, Appl. Phys. Lett. **90**, 162103 (2007).
24) X. Wang, S. B. Che, Y. Ishitani, and A. Yoshikawa, Appl. Phys. Lett. **90**, 151901 (2007).
25) X. Wang, S. B. Che, Y. Ishitani, and A. Yoshikawa, Jpn. J. Appl. Phys. **45**, L730 (2006).
26) A. Yoshikawa, X. Wang, Y. Ishitani, and A. Uedono, Phys. Status Solidi A **207**, 1011 (2010).
27) X. Wang, S. Liu, N. Ma, L. Feng, G. Chen, F. Xu, N. Tang, S. Huang, K. J. Chen, S. Zhou, and B. Shen, Appl. Phys. Express **5**, 015502 (2012).
28) M. Higashiwaki and T. Matsui, J. Cryst. Growth **251**, 494 (2003).
29) W. Gian, M. Skowronski, and G. S. Rohrer, MRS Proc. **423**, 475 (1996).
30) A. Zubrilov, *Properties of Advanced Semiconductor Materials: GaN, AlN, InN, BN, SiC, SiGe* (Wiley, New York, 2001) p. 49.
31) E. Dimakis, E. Iliopoulos, K. Tsagaraki, A. Adikimenakis, and A. Georgakilas, Appl. Phys. Lett. **88**, 191918 (2006).
32) K. Wang, T. Kosel, and D. Jena, Phys. Status Solidi C **5**, 1811 (2008).
33) I. Mahboob, T. D. Veal, L. F. J. Piper, C. F. McConville, H. Lu, W. J. Schaff, J. Furthmller, and F. Bechstedt, Phys. Rev. B **69**, 201307 (2004).
34) S. Mahanty, M. Hao, T. Sugahara, R. S. Q. Fareed, Y. Morishima, Y. Naoi, T. Wang, and S. Sakai, Mater. Lett. **41**, 67 (1999).

© 2016 The Japan Society of Applied Physics